SANDIA REPORT
SAND2019-15245
Printed November 2019

Sandia National Laboratories

A Concept for Platform Velocity Estimation Using a Multiphase Center Radar

Douglas L. Bickel

Prepared by
Sandia National Laboratories
Albuquerque, New Mexico
87185 and Livermore,
California 94550

Issued by Sandia National Laboratories, operated for the United States Department of Energy by National Technology & Engineering Solutions of Sandia, LLC.

Available to DOE and DOE contractors from
U.S. Department of Energy
Office of Scientific and Technical Information
P.O. Box 62
Oak Ridge, TN 37831

Telephone: (865) 576-8401
Facsimile: (865) 576-5728
E-Mail: reports@osti.gov
Online ordering: http://www.osti.gov/scitech

Available to the public from
U.S. Department of Commerce
National Technical Information Service
5301 Shawnee Rd
Alexandria, VA 22312

Telephone: (800) 553-6847
Facsimile: (703) 605-6900
E-Mail: orders@ntis.gov
Online order: https://classic.ntis.gov/help/order-methods/

ABSTRACT

An important part of a navigation system for a moving platform is the estimation of the rate of travel. This document presents a method for estimating the platform velocity in 3-dimensions using multiple antenna subarrays which could be used to augment navigation in a GPS-degraded environment. An advantage of this technique is that it does not require any knowledge of a positions of any landmarks.

Results from radar data collected by the Sandia National Laboratories demonstration radar system are presented to illustrate the promise of this technique.

ACKNOWLEDGEMENTS

The analysis work and document development were supported by the current Laboratory Directed Research and Development (LDRD) program at Sandia National Laboratories titled "SAR Image Formation and Feedback to Navigation Subsystem in GPS Denied and Degraded Environments", with Scott Jenkins as the principal investigator. In addition, the radar data used for in this report were from a system developed under the LDRD titled "Moving Target Detection and Location in Terrain Using Radar", which ran from October, 2012, through September, 2014. It was anticipated in the early stages of that LDRD that the radar would be used for several purposes, including this application, so data was collected in August, 2014, to test and expand upon previous hypotheses regarding motion measurement with multiple phase centers.

It is also acknowledged here that this work can be thought of as an extension of the work discussed in [1] which was partly a result of the Cooperative Research and Development Agreement (CRADA) between Sandia National Laboratories and General Atomics Aeronautical Systems, Inc. – CRADA SC08/01749.01.08.

Thanks to Jim Hudgens (former Sandian) for supporting the radar development for the system used for these tests. Thanks to Dale Dubbert (retired), Gil Delaplain (retired), David Harmony (retired), Kyle White (retired), Mark Learn, Scott Devonshire (retired), and others involved in the Ku-band FARAD system development. Thanks to Ted Kim, Doug Jordan (retired), Rick Naething and Robert Morris for helping to devise and support the flight test experiment used in this document and for generating the additional necessary software for the flight tests. Thanks to Armin Doerry and Rick Naething for brainstorming the concepts. Thanks to the current LDRD team members Scott Jenkins and Tim Bielek for technical interactions. Thanks to many other Sandia colleagues to whom I apologize for not listing you, but without whom this work would not be possible.

Finally, thanks to Volker Horndt from General Atomics, for your general technical curiosity in a variety of radar areas that led to your deep insights. When combined with your winsome personality, it was truly enjoyable to work with you. You are missed.

CONTENTS

LIST OF FIGURES

ACRONYMS, SYMBOLS, AND DEFINITIONS

Abbreviation	Definition
f_D	Doppler
λ	Radar wavelength
$\vec{V}$	Velocity vector
$\vec{u}_r$	Unit vector from the antenna phase center to the target
$\Delta\Phi_a$	Interferometric phase between azimuth phase centers
$\Delta\Phi_e$	Interferometric phase between elevation phase centers
B_a	Azimuth baseline length
B_e	Elevation baseline length
N	Number of samples used in the estimation of the velocity components

“There is no science without political science.”

Dr. Barry J. Geldzahler

1. INTRODUCTION

This document discusses the theory and application of a technique for estimating the 3-dimensional velocity of an airborne system using a multiple phase center radar system. This can be thought of as an extension of the technique discussed in [1]. Aside from presenting the background, relationship to other techniques, theory, and the extension to 3-dimensions, this document illustrates the utility by application to real flight test data collected with the Sandia Ku-band FARAD radar system.

We note that an important advantage of this method is that it does not require knowledge of any target locations.

1.1. Background

An important part of navigation of a system is to estimate the rate of travel. In many sensor systems, this information is provided by the inertial measurement unit (IMU) combined with the global positioning system (GPS) inputs. With the anticipated vulnerabilities in the GPS signals, and known bias and other errors in IMUs, particularly the more affordable systems, it is of interest to investigate other possible solutions.

This report discusses a potential component of such a solution that estimates the current velocity in 3D relative to the orientation of an antenna system. An advantage of this technique is that we do not rely on knowledge of any landmarks in the data sensed by the radar. It is envisioned that this is a possible tool among many where radar can be used in a GPS-degraded environment.

Interestingly, we will briefly note that this work can be shown have a relationship to an old radar navigation technique and can be thought of in some sense as the "inverse" of that technique.

1.2. Report organization

This report is organized to first present the background information above, followed by the basic concepts and theory in the next section. Section 3 describes an experiment and results of applying this technique to a data collected with Sandia's four phase-center Ku-band system. Section 4 presents errors and remaining issues to resolve. Section 5 briefly discusses potential future work. Finally, section 6 gives the conclusions.

"There is nothing so practical as a good theory."

Kurt Lewin

2. CONCEPTS AND THEORY

The basic concept is related to that presented previously in [1] and is described now. A radar essentially senses the range to various targets within a beam. Upon detecting a target, the radar system measures the time delay to the target which yields the range information to the target. In addition, in coherent radar systems, the range information is encoded in the far-field signal phase. The latter is typically considered much more sensitive to small changes. The change in this phase with geometry provides powerful information on the relative target geometry[1]. This phase information is important in other radar techniques, such as synthetic aperture radar, interferometric synthetic aperture radar, along-track interferometry, differential interferometry, and many others. The technique discussed in this document makes use of the range information encoded in the far-field phase[2], as well.

At a high level, one could think of this technique as using the differential Doppler information between antennas at known locations on the platform to estimate the velocities. This way of thinking reveals the relationship to traditional radar navigation methods. At another level, this technique can be thought of as using comparison between direction-of-arrival information between Doppler and interferometric radar to estimate the velocity components. This way of thinking is presented in the math that follows.

2.1. Basics and math

The basic math is presented here. The instantaneous Doppler of the radar sensed to a stationary target in a particular direction is given by:

$$f_D = \frac{2}{\lambda}\vec{V}\cdot\vec{u}_r \tag{1}$$

We note from equation (1) that if we can get enough angular diversity from multiple target directions, i.e., multiple different $\vec{u}_r$ values, then given the radar's ability to measure Doppler, f_D, we can invert and solve for the velocity vector, $\vec{V}$. This is precisely what this technique does. Note that finer wavelengths, λ, provide us the potential for better velocity sensitivity[3].

In general, we can represent a series of Doppler measurements in equation (1) in matrix form as follows:

[1] In this report, we are interested in the temporal angular change of the radar encoded in the phase changes, which manifests in Doppler. Implicit is a good knowledge of the pulse repetition frequency.

[2] We note that we will discuss in terms of interferometric techniques in this document, but monopulse techniques could be used just as well, as was discussed in [1].

[3] This higher sensitivity also means that we must maintain a higher fidelity radar system, because we are also more sensitive to system errors such as calibration, radome errors, etc.

$$\begin{bmatrix} f_{D,1} \\ f_{D,2} \\ \bullet \\ \bullet \\ \bullet \\ f_{D,N} \end{bmatrix} = \frac{2}{\lambda} \begin{bmatrix} \left(\vec{u}_{r1} \cdot \vec{u}_i\right) & \left(\vec{u}_{r1} \cdot \vec{u}_j\right) & \left(\vec{u}_{r1} \cdot \vec{u}_k\right) \\ \left(\vec{u}_{r2} \cdot \vec{u}_i\right) & \left(\vec{u}_{r2} \cdot \vec{u}_j\right) & \left(\vec{u}_{r1} \cdot \vec{u}_k\right) \\ \bullet & \bullet & \bullet \\ \bullet & \bullet & \bullet \\ \bullet & \bullet & \bullet \\ \left(\vec{u}_{rN} \cdot \vec{u}_i\right) & \left(\vec{u}_{rN} \cdot \vec{u}_j\right) & \left(\vec{u}_{rN} \cdot \vec{u}_k\right) \end{bmatrix} \begin{bmatrix} v_i \\ v_j \\ v_k \end{bmatrix} \tag{2}$$

where $f_{D,n}$, is the n^{th} observed Doppler, and $\left(\vec{u}_i, \vec{u}_j, \vec{u}_k\right)$ are unit vectors in a chosen orthogonal coordinate system that we will discuss more later. The 3-tuple $\left(v_i, v_j, v_k\right)$ are the velocity vector components to be estimated in the chosen coordinate. In other words:

$$\begin{aligned} v_i &= \vec{V} \cdot \vec{u}_i \\ v_j &= \vec{V} \cdot \vec{u}_j \\ v_k &= \vec{V} \cdot \vec{u}_k \end{aligned} \tag{3}$$

Let:

$$\vec{f}_{D,meas} = \begin{bmatrix} f_{D,1} \\ f_{D,2} \\ \bullet \\ \bullet \\ \bullet \\ f_{D,N} \end{bmatrix}$$

$$\mathbf{U} = \begin{bmatrix} \left(\vec{u}_{r1} \cdot \vec{u}_i\right) & \left(\vec{u}_{r1} \cdot \vec{u}_j\right) & \left(\vec{u}_{r1} \cdot \vec{u}_k\right) \\ \left(\vec{u}_{r2} \cdot \vec{u}_i\right) & \left(\vec{u}_{r2} \cdot \vec{u}_j\right) & \left(\vec{u}_{r1} \cdot \vec{u}_k\right) \\ \bullet & \bullet & \bullet \\ \bullet & \bullet & \bullet \\ \bullet & \bullet & \bullet \\ \left(\vec{u}_{rN} \cdot \vec{u}_i\right) & \left(\vec{u}_{rN} \cdot \vec{u}_j\right) & \left(\vec{u}_{rN} \cdot \vec{u}_k\right) \end{bmatrix} \tag{4}$$

$$\vec{V} = \begin{bmatrix} v_i \\ v_j \\ v_k \end{bmatrix}$$

where $\vec{f}_{D,meas}$ is an N by 1 vector of the Doppler measurements, $\mathbf{U}$ is a 3 by N matrix of direction cosine measurements corresponding to the Doppler measurements, and $\vec{V}$ is an 3 by 1 velocity estimate vector. Equation (2) can be rewritten as:

$$\mathbf{U}\vec{V} = \frac{\lambda}{2}\vec{f}_{D,meas} \tag{5}$$

If $N = 3$ then $\mathbf{U}$ is a square matrix and can be inverted, provided it is not singular. Often in practice, $N > 3$ in which case we have an overdetermined system and must solve by pseudoinverse techniques (see for example [2]):

$$\begin{aligned} \left(\mathbf{U}^T\mathbf{U}\right)\vec{V} &= \frac{\lambda}{2}\mathbf{U}^T\vec{f}_{D,meas} \\ \vec{V} &= \frac{\lambda}{2}\mathbf{U}^\dagger\vec{f}_{D,meas} = \frac{\lambda}{2}\left(\mathbf{U}^T\mathbf{U}\right)^{-1}\mathbf{U}^T\vec{f}_{D,meas} \end{aligned} \tag{6}$$

where $\mathbf{U}^\dagger$ is typically is referred to as the pseudo-inverse of matrix $\mathbf{U}$.

Equation (6) is the key to what we are doing in this document. This equation tells us a few things: 1) we desire many good measurements of the Doppler; 2) we require corresponding angle information for each Doppler measurement to generate $\mathbf{U}$; and 3) we desire a good spread of angles over the range-Doppler image so that $\mathbf{U}$ is reasonably well-conditioned..

2.2. Phase centers and velocity measurement

In order to solve the above equation, we need information to fill in the matrix $\mathbf{U}$. The technique presented in this document uses information derived from phase centers separated along each the azimuth and elevation directions. This information provides the angle measurements used in $\mathbf{U}$. Obviously, the angle measurements provided by the antenna are relative to the coordinates that contain the antenna phase centers. The specifics of the system used in the experiment is presented later in this report.

The antenna coordinates in this document are $\left(\vec{u}_a, \vec{u}_n, \vec{u}_e\right)$ which means that we let:

$$\begin{aligned} \vec{u}_i &= \vec{u}_a \\ \vec{u}_j &= \vec{u}_n \\ \vec{u}_k &= \vec{u}_e \end{aligned} \tag{7}$$

where $\vec{u}_a$ is a unit vector along the baseline between the azimuth antenna phase centers in the azimuth ("along-track") direction, $\vec{u}_n$ is the unit vector normal to the plane containing the antenna phase centers ("line-of-sight"); and $\vec{u}_e$ is the unit vector along the baseline between the elevation phase centers. Note that $\vec{u}_e$ was not considered in [1].

The result is the matrix $\mathbf{U}$ becomes:

$$\mathbf{U} = \begin{bmatrix} (\vec{u}_{r1} \cdot \vec{u}_a) & (\vec{u}_{r1} \cdot \vec{u}_n) & (\vec{u}_{r1} \cdot \vec{u}_e) \\ (\vec{u}_{r2} \cdot \vec{u}_a) & (\vec{u}_{r2} \cdot \vec{u}_n) & (\vec{u}_{r1} \cdot \vec{u}_e) \\ \bullet & \bullet & \bullet \\ \bullet & \bullet & \bullet \\ \bullet & \bullet & \bullet \\ (\vec{u}_{rN} \cdot \vec{u}_a) & (\vec{u}_{rN} \cdot \vec{u}_n) & (\vec{u}_{rN} \cdot \vec{u}_e) \end{bmatrix} \tag{8}$$

If we let the unit vector, $\vec{u}_{r,n}$, be the direction from the center of the antenna to the n^{th} target within the range-Doppler image scene, then we can estimate the components in equation (8) as follows:

$$\begin{aligned} \vec{u}_a \cdot \vec{u}_{r,n} &= \frac{\lambda}{2\pi B_a} \Delta\Phi_{a,n} \\ \vec{u}_e \cdot \vec{u}_{r,n} &= \frac{\lambda}{2\pi B_n} \Delta\Phi_{e,n} \end{aligned} \tag{9}$$

where λ is the radar wavelength, B_a is the azimuth baseline (phase center separation) length, B_e is the elevation baseline length, $\Delta\Phi_{a,n}$ is the interferometric phase between the azimuth phase center corresponding to the n^{th} target within the range-Doppler image, and $\Delta\Phi_{e,n}$ is the interferometric phase between the elevation phase centers for the n^{th} target within the range-Doppler image. The final direction cosine value we need is $\vec{u}_n \cdot \vec{u}_{r,n}$, and comes from use of the Pythagorean theorem and the fact that we are dealing with a unit vector.

In this document we will assume that the beamwidths are small such that we can linearize the values in $\mathbf{U}$. This means that both $\vec{u}_a \cdot \vec{u}_{r,n}$ and $\vec{u}_e \cdot \vec{u}_{r,n}$ will be small, and that $\vec{u}_n \cdot \vec{u}_{r,n} \approx 1$. Note that because we have defined our velocity coordinates along the natural antenna coordinates, these values for the direction cosines of the angles are limited by the beamwidths in azimuth and elevation. We will note later that we need some diversity in azimuth and elevation angles within the data in $\mathbf{U}$ in order to limit errors in the velocity estimation.

The result of the approximations is:

$$\mathbf{U} \approx \begin{bmatrix} (\vec{u}_{r1} \cdot \vec{u}_a) & 1 & (\vec{u}_{r1} \cdot \vec{u}_e) \\ (\vec{u}_{r2} \cdot \vec{u}_a) & 1 & (\vec{u}_{r1} \cdot \vec{u}_e) \\ \bullet & \bullet & \bullet \\ \bullet & \bullet & \bullet \\ \bullet & \bullet & \bullet \\ (\vec{u}_{rN} \cdot \vec{u}_a) & 1 & (\vec{u}_{rN} \cdot \vec{u}_e) \end{bmatrix} \tag{10}$$

Under these assumptions, the solution for the velocity vector components in equation (6) becomes a least-squares fit of a plane in 3D space. The equation should follow a solution that is of the form:

$$\frac{\lambda}{2} f_{D,n} = \vec{V} \cdot \vec{u}_n + \left(\vec{V} \cdot \vec{u}_a\right)\left(\vec{u}_a \cdot \vec{u}_{r,n}\right) + \left(\vec{V} \cdot \vec{u}_e\right)\left(\vec{u}_e \cdot \vec{u}_{r,n}\right) = v_n + v_a\left(\vec{u}_a \cdot \vec{u}_{r,n}\right) + v_e\left(\vec{u}_e \cdot \vec{u}_{r,n}\right) \tag{11}$$

where the line-of-sight velocity term, v_n, acts as an intercept/offset (i.e., bulk line-of-sight) term, and v_a and v_e act as slope terms.

To show that this is a 3D plane equation, we rewrite the above equation as:

$$v_a\left(\vec{u}_a \cdot \vec{u}_{r,n}\right) + v_e\left(\vec{u}_e \cdot \vec{u}_{r,n}\right) + \left(v_n - \frac{\lambda}{2} f_{D,n}\right) = 0 \tag{12}$$

From this form of the equation, we can recognize that the normal vector to the plane is $\left(v_a, v_e, 1\right)$ whose coordinates are the values $\left(\vec{u}_a \cdot \vec{u}_{r,n}\right)$, $\left(\vec{u}_e \cdot \vec{u}_{r,n}\right)$, and $\frac{\lambda}{2} f_{D,n}$, respectively. The result is that our least-squares solution is estimating the normal to the plane, subject to the vector constraint of $\left(0,0,1\right)$ in the normalized-Doppler direction, and also estimating the offset of the plane in the normalized-Doppler direction.

Similar to [4], we can use the first line of equation (6) along with equation (10) to write the 3D plane least-squares fit as:

$$\begin{bmatrix} \sum_{n=1}^{N}\left(\vec{u}_{r,n} \cdot \vec{u}_a\right)^2 & \sum_{n=1}^{N}\left(\vec{u}_{r,n} \cdot \vec{u}_a\right) & \sum_{n=1}^{N}\left(\vec{u}_{r,n} \cdot \vec{u}_a\right)\left(\vec{u}_{r,n} \cdot \vec{u}_e\right) \\ \sum_{n=1}^{N}\left(\vec{u}_{r,n} \cdot \vec{u}_a\right) & N & \sum_{n=1}^{N}\left(\vec{u}_{r,n} \cdot \vec{u}_e\right) \\ \sum_{n=1}^{N}\left(\vec{u}_{r,n} \cdot \vec{u}_a\right)\left(\vec{u}_{r,n} \cdot \vec{u}_e\right) & \sum_{n=1}^{N}\left(\vec{u}_{r,n} \cdot \vec{u}_e\right) & \sum_{n=1}^{N}\left(\vec{u}_{r,n} \cdot \vec{u}_e\right)^2 \end{bmatrix} \begin{bmatrix} v_a \\ v_n \\ v_e \end{bmatrix} = \left(\frac{\lambda}{2}\right) \begin{bmatrix} \sum_{n=1}^{N}\left(\vec{u}_{r,n} \cdot \vec{u}_a\right) f_{D,n} \\ \sum_{n=1}^{N} f_{D,n} \\ \sum_{n=1}^{N}\left(\vec{u}_{r,n} \cdot \vec{u}_e\right) f_{D,n} \end{bmatrix} \tag{13}$$

2.3. Algorithm basics

This section considers the algorithm implementation. Essentially the algorithm proceeds as shown in the flow chart in Figure 2 in [1] so we will not repeat the drawing here. The main difference is that the least squares is generalized to a 3-dimensional curve (plane), rather than a 2-dimensional line as discussed in [1].

2.4. Algorithm considerations

This section presents several algorithm considerations. One benefit of this algorithm is that we do not need to know where the area that we are imaging is located. Also, natural clutter works well for this application. Man-made objects and radar reflectors are not required in the scene.

Another consideration is the appropriateness of the data within the scene. In this implementation, we cull the data that we use in estimation for signal-to-noise ratio (SNR). In interferometric radar imaging, the magnitude of the coherence carries information about the phase variance which is often mostly affected by the SNR.

Moving targets could affect the performance. This method will not work well over the ocean. Note that we might want to cull for moving targets if we suspect that this might be an issue.

Another issue with this method is that the use of multiple phase centers requires much more careful system calibration than those which use only a single phase center/antenna pattern. We will not say much more in this document about the calibration process, other than to state that this was actually the most challenging part of work for obtaining the experimental radar results.

Note that for best performance we want to orient the antenna along main flight direction.

2.5. Relationship to other concepts

In this section we discuss a relationship of this technique to a technique from the 1960s referred to as radar Doppler navigation which is discussed in [3] among other references. The Doppler navigation method has even been migrated to sonar applications. The Doppler navigation concept solves the same equation, equation (5), but it generates the values in $\mathbf{U}$ differently. In the method described in this report, we use multiple phase centers to estimate the values in $\mathbf{U}$ by a single "beam" with a small to modest beamwidth. The angle diversity in $\mathbf{U}$ required to solve for the velocities is generated by a large angular separation (i.e., squinting) of beams on the platform using a single phase center.

In the traditional Doppler navigation method, the angle diversity in $\mathbf{U}$ is generated by physically pointing multiple (usually 3 to 4) small beams in greatly different directions. Figure 1 shows a couple different options, where the 4 beam technique shown in Figure 1b was referred to as "Janus". Note that the beams have essentially the same antenna phase center but are pointed in quite different directions. The angular information derives from the power centroid of the returns from the various beams. Each of the beam directions are fixed with respect to the platform. Beam directions and angles will be influenced by terrain. The Janus configuration was used because it simplifies some of the math in the equations above. As with the method suggested in this document, moving scenes such as the ocean disturb the velocity estimate results.

There are similarities and differences between the method proposed here, and the traditional Doppler navigation. In some ways, one might think of the method proposed in this document as an inverse Doppler navigation, since it relies on separation of the beams on the aircraft rather than separation of beams on the scene.

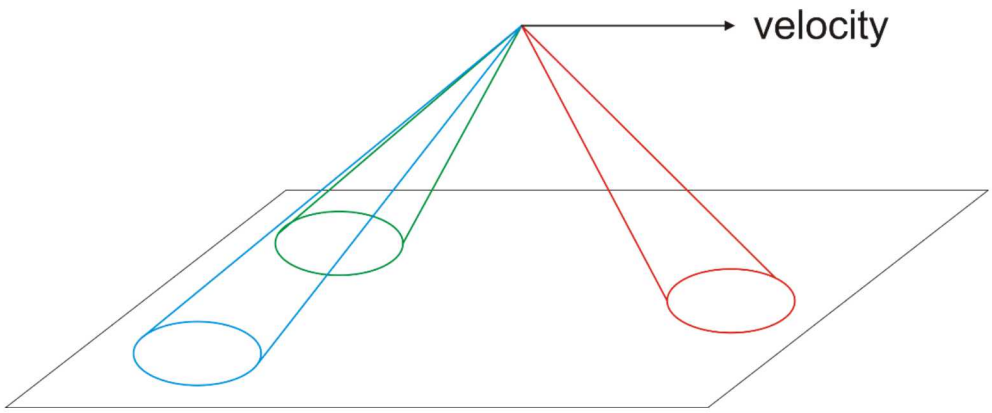

Figure 1a. Three beam example for Doppler navigation

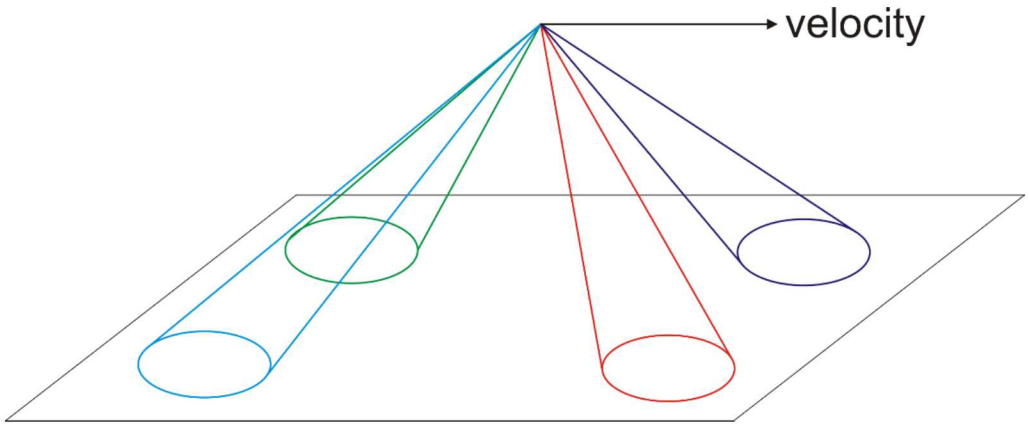

Figure 1b. Four beam ("Janus") example for Doppler navigation

3. EXPERIMENT DESCRIPTION AND RESULTS

This section of the document discusses the experimental results from data collected with the Sandia Ku-band FARAD radar system.

3.1. System description

The radar system used to collect this data is a four-phase center Ku-band radar developed from 2011 to 2014 for a Laboratory Directed Research and Development (LDRD) effort. The application of this type of multiple phase center radar to the problem described here in this document had been anticipated even prior to 2011. The result was that the experiment described below was flown at the tail end of the LDRD effort.

Figure 2 shows the antenna for the system used to collect this data. It has two phase centers oriented in elevation, and three phase centers oriented in the along-track direction[4]. The four phase centers are labeled A1 through A4 and can be multiplexed in any order or combination into either 2 or 1 RF channel(s). For this experiment the phase difference between A1 and A4 are used to estimate the in equation (9) to estimate $\vec{u}_e \cdot \vec{u}_{r,n}$. Likewise, A2, A3, and A4 are used to estimate $\vec{u}_a \cdot \vec{u}_{r,n}$.

3.2. Experiment description

The experimental data used in the analysis below is now described. The Ku-band FARAD system was flown in August 2014 using a circle collection mode of an area on Kirtland Airforce Base that contains a formerly used outdoor antenna range with an inverted concrete vee. The area is often used for airborne radar testing and contain a set of radar reflectors, although *no knowledge* of the reflector locations was used in this processing and analysis[5]. The data was collected for all four phase centers. The SAR image from one of phase centers of the first patch of the circle is shown in Figure 3.

[4] One of the phase centers is shared between elevation and along-track.

[5] In fact, no knowledge of the position of anything in the scene is required, nor are reflectors required within the scene for this technique to work.

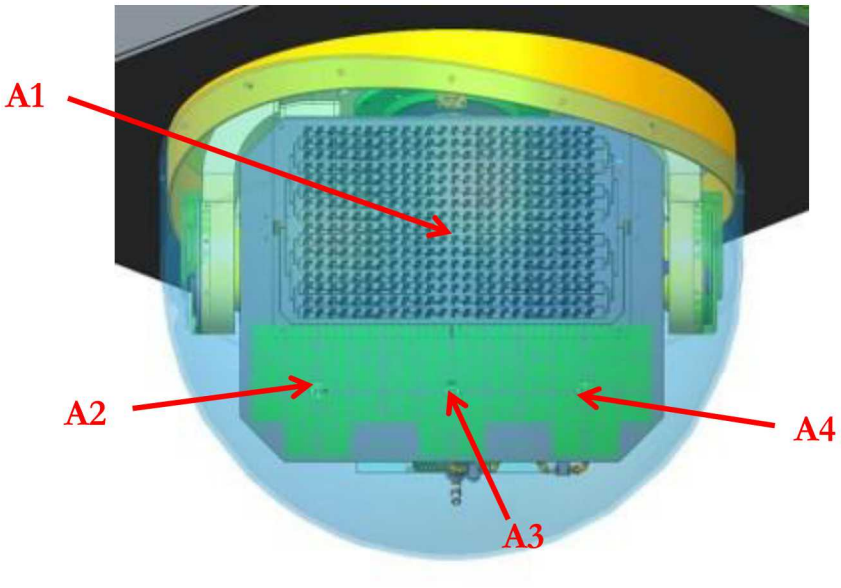

Figure 2. Antenna for Ku-band FARAD system

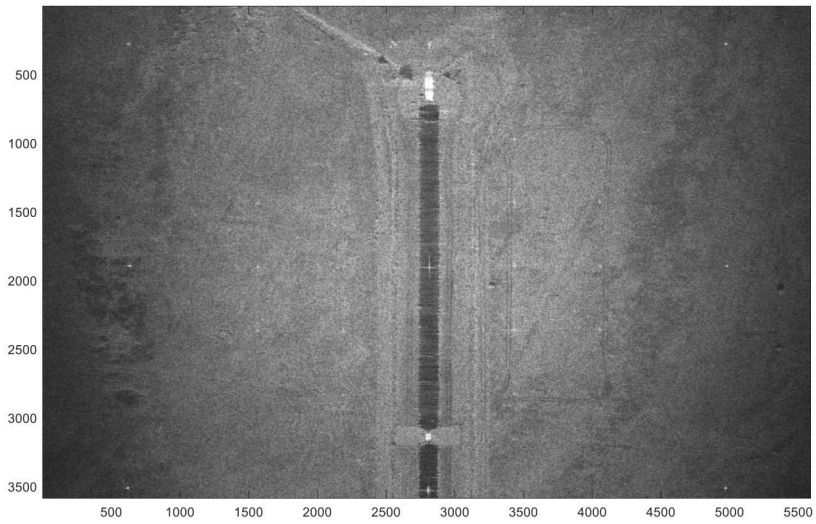

Figure 3. First SAR image patch in the circle of the area imaged in circular geometry (shown without injected errors)

For our experiment, we flew three complete circles around the target area. The boresight of the antenna was maintained on the center of the scene and the antenna is kept during each of the circle collects. The radar is actually flying very close to broadside to the scene center at all times.

For the circle data collection mode, an x and y-direction are chosen in the horizontal plane, with the z-direction being in the vertical at the scene center. The x-direction is fixed for the entire circle in a direction which was approximately the flight direction with respect to true north upon entering the circle. This direction was the same for all circles, which was nearly due east.

For the first circle, the motion measurement operates normally with no errors purposely introduced. For the second circle, the motion measurement injects an error into the reported radar coordinate in the *x*-direction. The error is a 45 m offset with a 0.25 m/s change in *x*-position. In the third circle, the *x*-error injected into the report reported motion measurement metadata is a 90 m offset with a 0.5 m/s changing *x*-position error. The hypothesis is that we can estimate the true 3-D velocity using the multiple phase centers in the face of these falsely reported changing position errors.

The fact that the *x*-direction is fixed with respect true north during the entire circle means that as we fly around the target area the radar along-track, elevation, and line-of-sight directions change during the circle. So we witness what appears to be changing velocities errors *from the radar's perspective*. Figure 4 illustrates the approximate errors introduced for the second case where the *x*-position error is a 45 m offset with changing at a rate of 0.25 m/s[6]. Figure 5 illustrates the approximate errors introduced for the third case where the *x*-position error is a 90 m offset with a changing at a rate of 0.5 m/s[7].

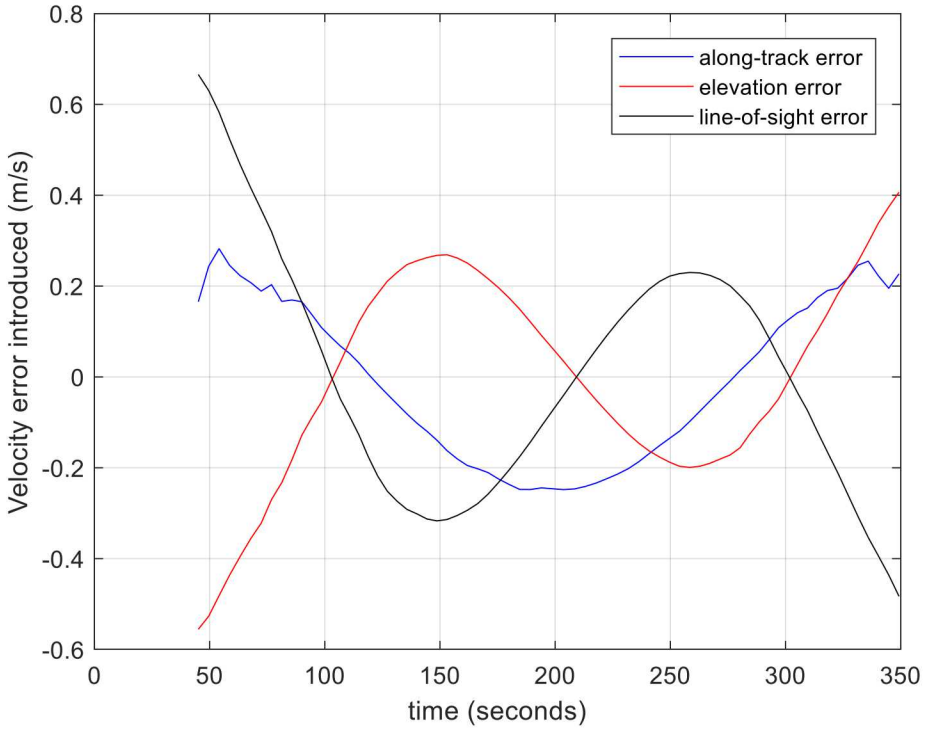

Figure 4. Velocity errors in the radar motion measurement directions by injecting a false 45 m offset and 0.25 m/s into the x-position error

[6] Note that the errors will at times be larger than 0.25 m/s because the initial position offset error of 45 m causes the projection direction of the line-of-sight to be wrong. In other words, the radar thinks there is a squint when in fact it is actually always flying broadside to the target area. This projection changes during the circle as well because of the 0.25 m/s velocity error introduced.

[7] Same comment as the previous on applies on apparent larger than 0.5 m/s errors due to the 90 m offset.

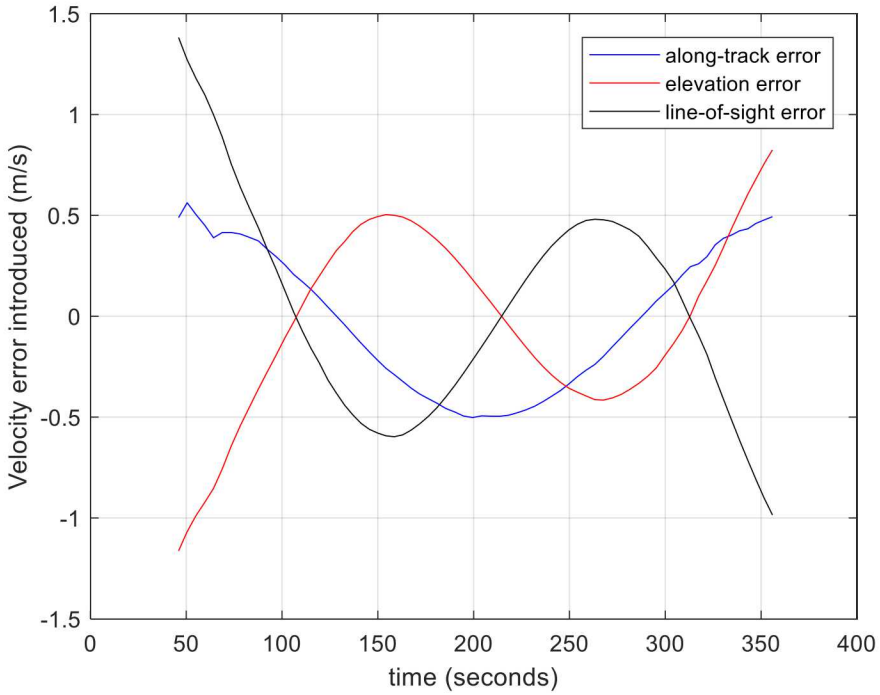

Figure 5. Velocity errors in the radar motion measurement directions by injecting a false 90 m offset and 0.5 m/s into the x-position error

Note that the errors will cause differing levels of shifts and misfocus within the range-Doppler images as a function of the circle aspect angle.

3.3. Discussion of analysis

In this section we discuss some pertinent factors in our analysis of the data.

The coherent processing interval (CPI) used in this document to estimate the velocities is about 0.45 seconds long. Note that in theory longer integration times can theoretically yield better results – interestingly because of more data points and not because of improved signal-to-noise ratio. There is a practical limit due to loss of focus. We chose this length CPI to illustrate that we could get reasonable results with a sub-second lag time. However, to speed up processing we only processed and show an estimate once every 10 CPIs or about once every 4.5 seconds. There is nothing to stop us from estimating continuously from back-to-back CPIs every 0.45 seconds. This was just a fielder's choice, so to speak.

We mentioned above that we wanted to cull the data to avoid using noisy data in our estimates. We said that we used the magnitude of the coherence estimate between the phase centers as our metric. In accordance with this discussion, we chose to only use data in the matrix $\mathbf{U}$ where the coherence was greater than 0.9 coherence for both along track and elevation baselines. This choice was not optimized in any manner. In practice, we may want to assess what value works best for this application. We will discuss this somewhat in the error analysis in a later section.

3.4. Discussion of results

In this section we present the results of the analysis of the experimental data using the multiple phase centers to estimate the velocities. We will show the results from the three circles: the first circle, with no errors introduced; the second circle with 0.25 m/s error introduced; and the third circle with the 0.5 m/s error introduced. As a recap, recall that the second circle introduces a changing position error in nearly the east direction that is -45 m plus an increasing (nearly) east error of 0.25 m/s as the circle progresses. Likewise, the third circle introduces a changing position error in nearly the east direction of -90 m with an increasing nearly east error of 0.5 m/s as the circle progresses.

We provide a bit more description of the data and the analysis at this point. The roughly 6 minutes of time scale shown as the abscissa in the figures below represents essentially the whole circle. There is actually a short time at the beginning of the circle that we do not use due to an error introduced. It is believed that this is an initial antenna attitude error at the beginning of the pass that occurs while the antenna pointing is being initialized. This could theoretically be corrected but we have chosen not to in this analysis for convenience and clarity.

The first example we show is that estimate of the velocities in the case where no error is introduced into the motion measurement data. Figure 6 shows the line-of-sight velocity component, v_n, estimated using the multiple phase centers and the versus the truth. The residual estimate error is shown in Figure 7. The mean of these errors is -0.005 m/s and the standard deviation is 0.0067 m/s.

We look at the along-track velocity, v_a, estimate in Figure 8 and Figure 9, where Figure 8 shows the estimate versus truth and Figure 9 shows the difference in these curves as the error in the estimate. In this case for this velocity component the mean error is about -0.0035 m/s and the standard deviation is 0.026 m/s.

The estimated elevation, or out-of-plane, velocity, v_e, is shown in Figure 10 and the error in the estimate is shown in Figure 11. For this velocity component there is a mean error of is 0.0025 m/s and the standard deviation of the error is 0.043 m/s in this case.

We now proceed to the case where the 0.25 m/s error was introduced into the data. Figure 12 shows the estimated v_n value (blue curve) in this case versus the truth (red dashed curve). We have superimposed the false value (truth with the injected error) reported by motion measurement (black dashed curve). Figure 13 shows two error curves. The red curve is error caused by the false information we have injected into motion measurement, i.e., it is the black dashed curve minus the red dashed curve from Figure 12. The blue curve in Figure 13 is the error in the estimate of v_n, i.e., it is the blue curve minus the red dashed curve from error from Figure 12. The mean error in the estimate (blue curve in Figure 13) is -0.003 m/s and the standard deviation is 0.011 m/s in this case.

The estimated value of the along-track velocity, v_a ,for this same injected error case is presented in Figure 14. Again, in the figure we show the estimate, the truth, and the (false) value reported by motion measurement. Like before, we show the error in the reported motion measurement value (red curve), and the error in the estimate from out method (blue curve) on the same plot in Figure 15. The mean error of the blue curve is about -4.4×10^{-4} m/s and the standard deviation is 0.029 m/s.

Finally, for this injected error we look at the elevation velocity, v_e. Figure 16 shows the estimated v_e, along with the true value and the one reported by motion measurement[8]. Figure 17 shows the residual estimate error, and the error injected into the motion data. The mean error in the estimate is 0.01 m/s and the standard deviation is 0.048 m/s.

Lastly, we consider the third circle where we doubled the injected error from the case just mentioned, to a 90 m offset and a 0.5 m/s changing *x*-position error. Figure 18 shows the v_n, the estimated value, the truth, and the false reported value. Figure 19 shows the error in v_n that the injected error would cause versus the error in the estimate using the multiple phase centers. The mean error of the estimate of v_n in this case is -0.0049 m/s, and the standard deviation of this error is 0.010 m/s.

For this injected error, the plot of v_a for the estimate, the truth, and the value caused by the injected error is shown in Figure 20. Figure 21 shows the error in the estimate versus the error in the reported v_a value. The mean estimate error for this case is, 0.009 m/s and the standard deviation of the error is 0.022 m/s.

We show the v_e for this case with the 90 m offset and a 0.5 m/s changing position error injected. As before, Figure 22 shows the truth, the estimate, and the value with the injected error, and Figure 23 shows the error in the estimate for v_e for this case versus the error injected into the v_e value. The mean error is 5.4×10^{-4} m/s and the standard deviation for this case is 0.047 m/s.

[8] At this point we must admit a lingering issue. The radar was setup to perform real-time motion compensation via waveform adjustment based upon the falsified information injected into the motion measurement data. The first step in this processing is to remove this correction and then estimate the true velocity from using the multiple phase centers. Currently there is a constant scale error that is occurring when trying to remove the error that effects the estimate of v_e. The results shown for the 0.25 m/s and 0.5 m/s cases for v_e only have used a correction for this scaling error. We are still searching for the source of this error. Neither v_a nor v_n exhibit this scaling error, nor did the estimate of v_e when the falsified motion compensation is not present.

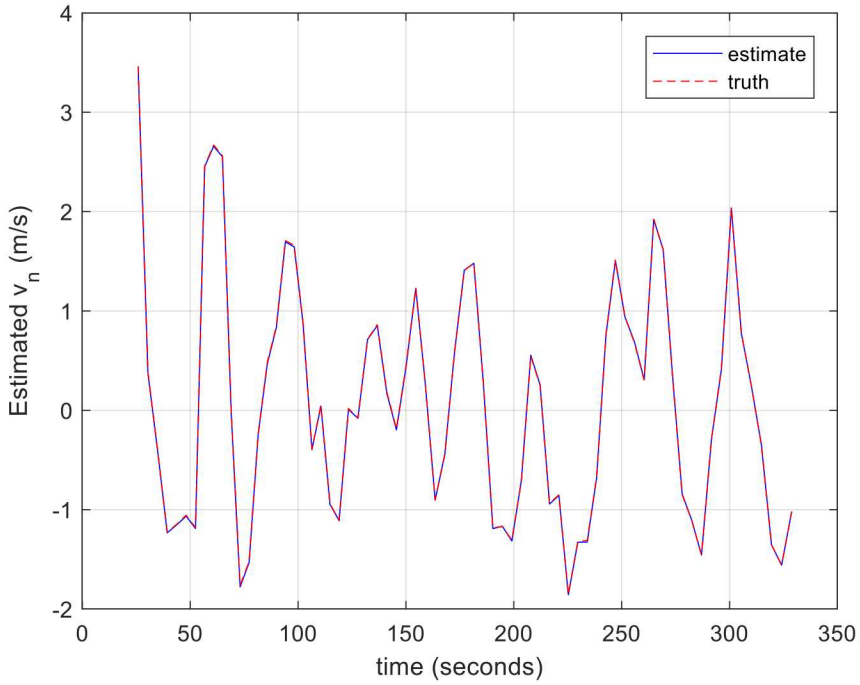

a

Figure 6. Estimate v_n of the line-of-sight velocity versus truth for case where no error is introduced into the motion measurement

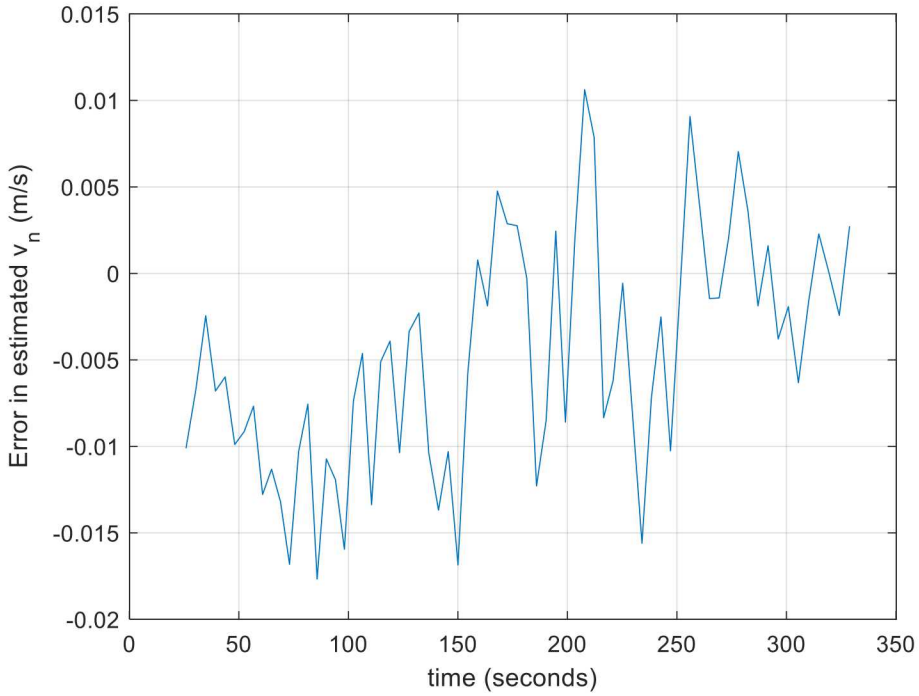

Figure 7. Error in estimate of v_n for case where no error is introduced into the motion measurement

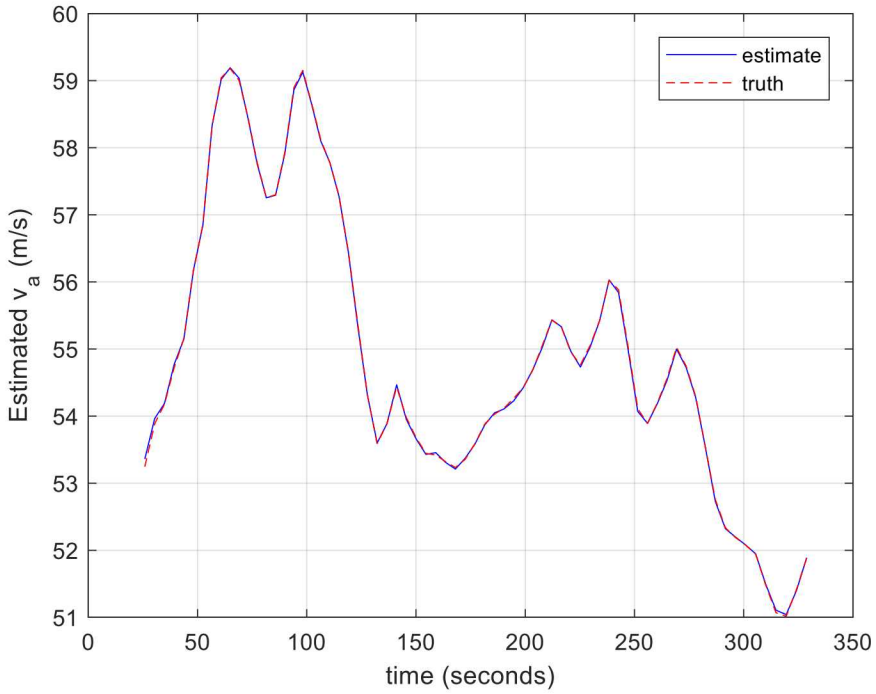

Figure 8. Estimate v_a of the along-track velocity versus truth for case where no error is introduced into the motion measurement

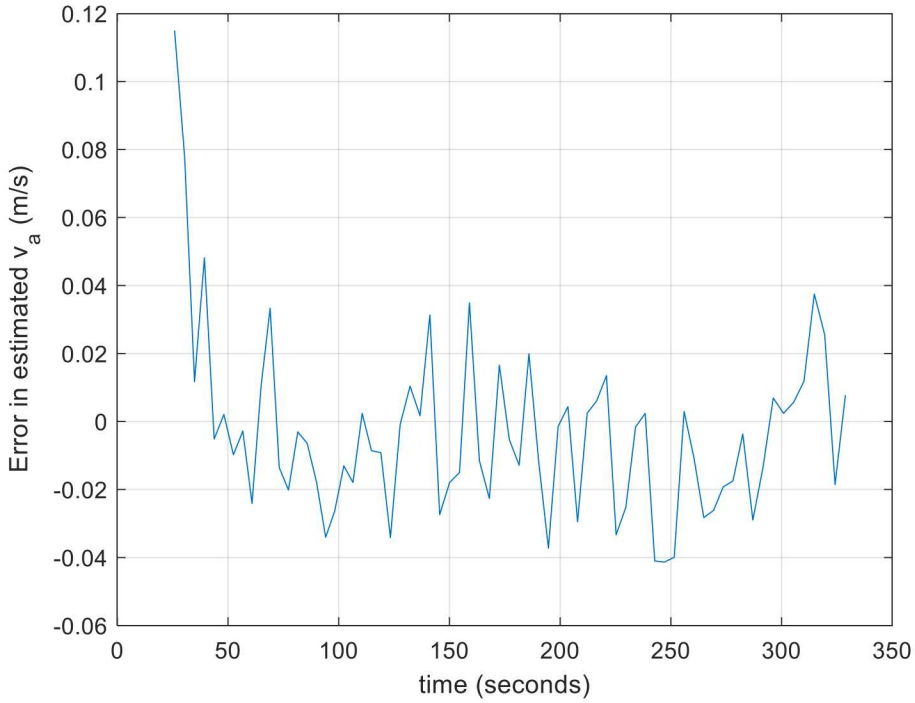

Figure 9. Error in estimate of v_a for case where no error is introduced into the motion measurement

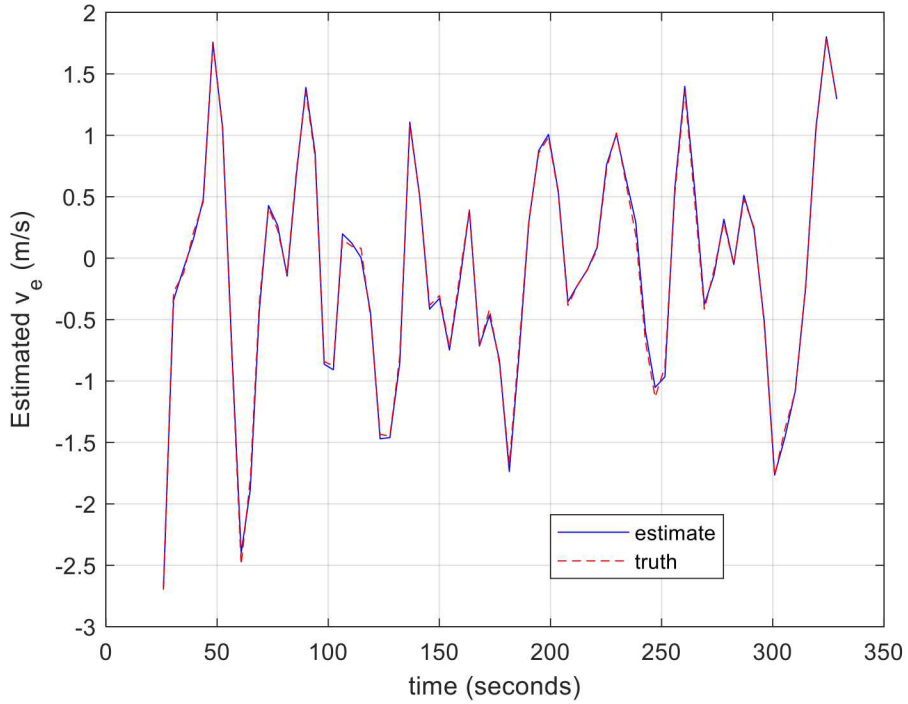

Figure 10. Estimate v_e of the elevation velocity versus truth for case where no error is introduced into the motion measurement

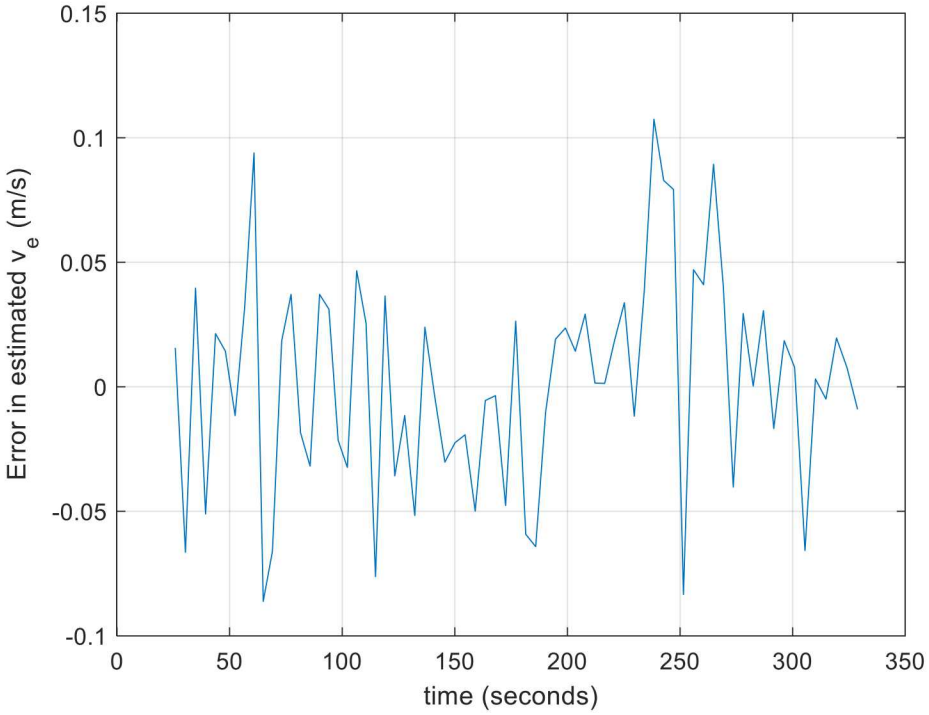

Figure 11. Error in estimate of v_e for case where no error is introduced into the motion measurement

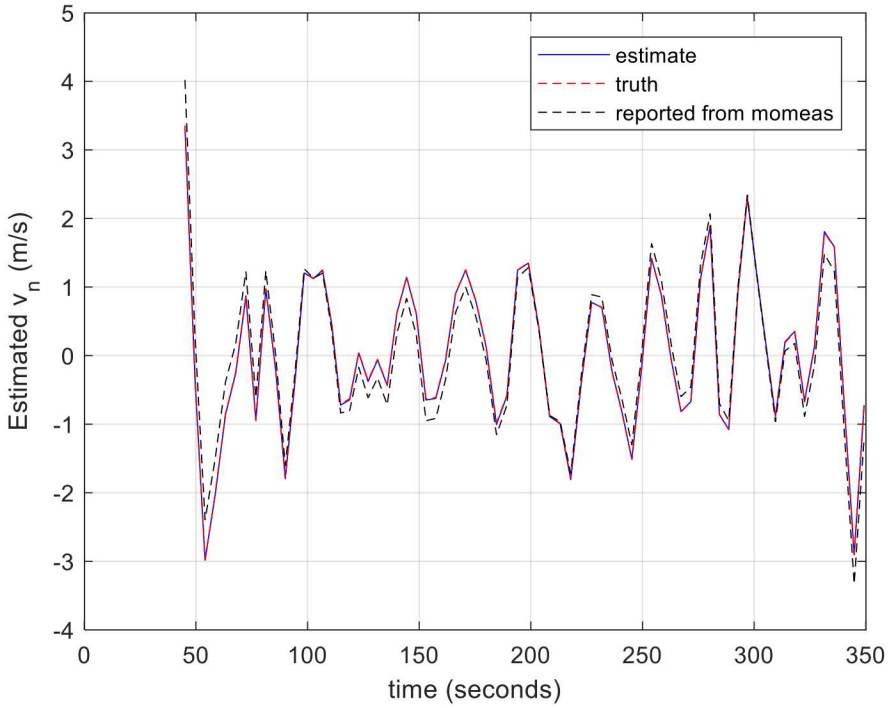

Figure 12. Estimate of v_n versus truth for case where 45 m offset and 0.25 m/s error is introduced into the reported motion measurement data

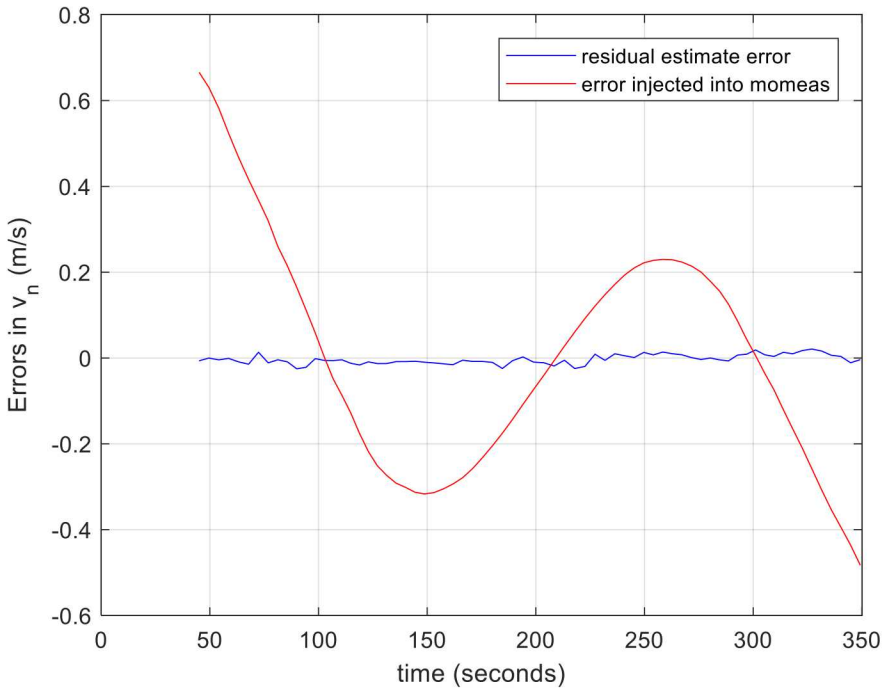

Figure 13. Injected motion measurement error in v_n caused by 45 m offset and 0.25 m/s error versus residual error in multiphase center v_n estimate

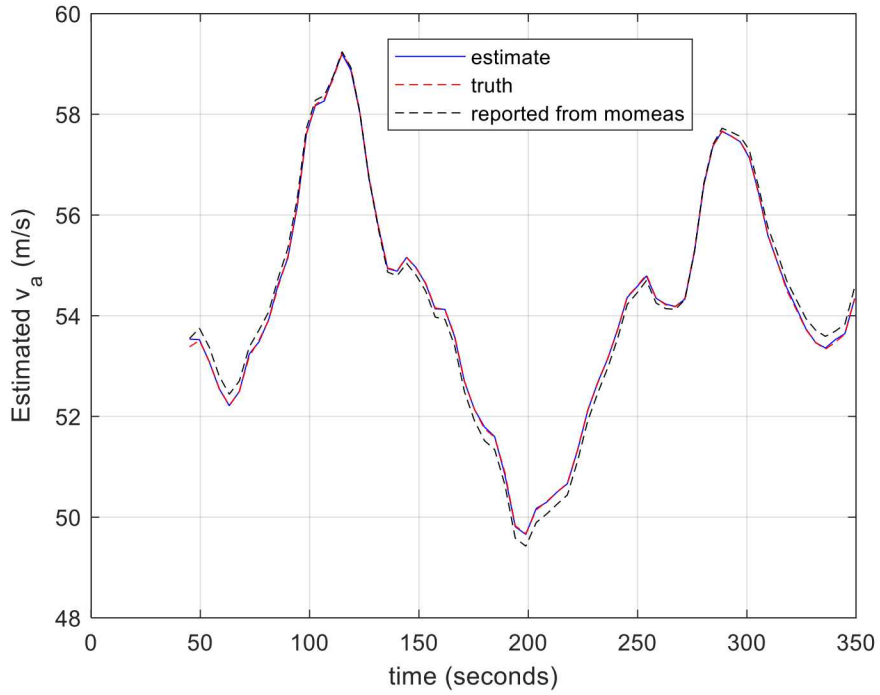

Figure 14. Estimate of v_a versus truth for case where 45 m offset and 0.25 m/s error is introduced into the reported motion measurement data

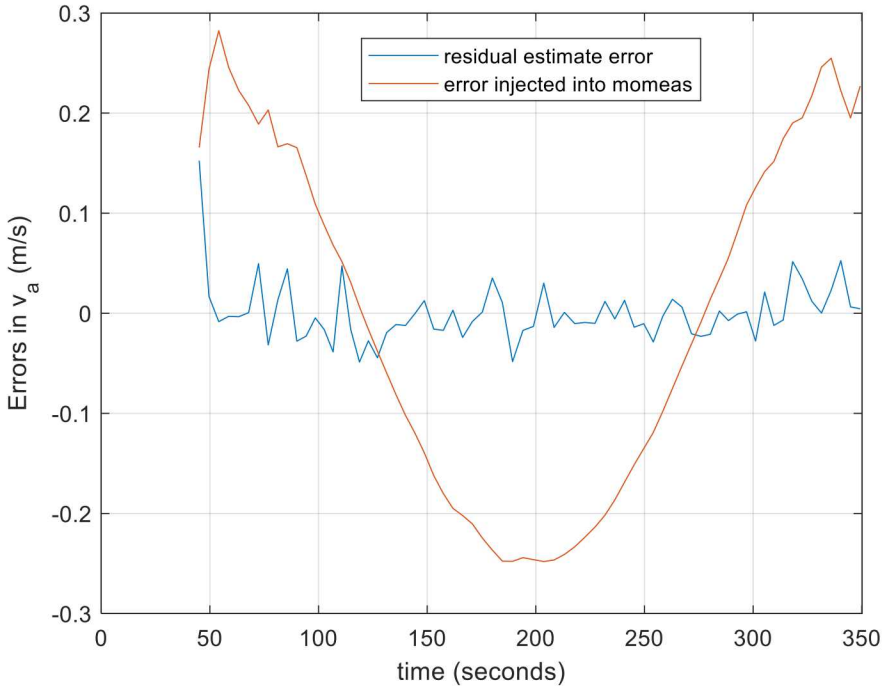

Figure 15. Injected motion measurement error in caused by v_a 45 m offset and 0.25 m/s error versus residual error after multiphase center v_a estimate

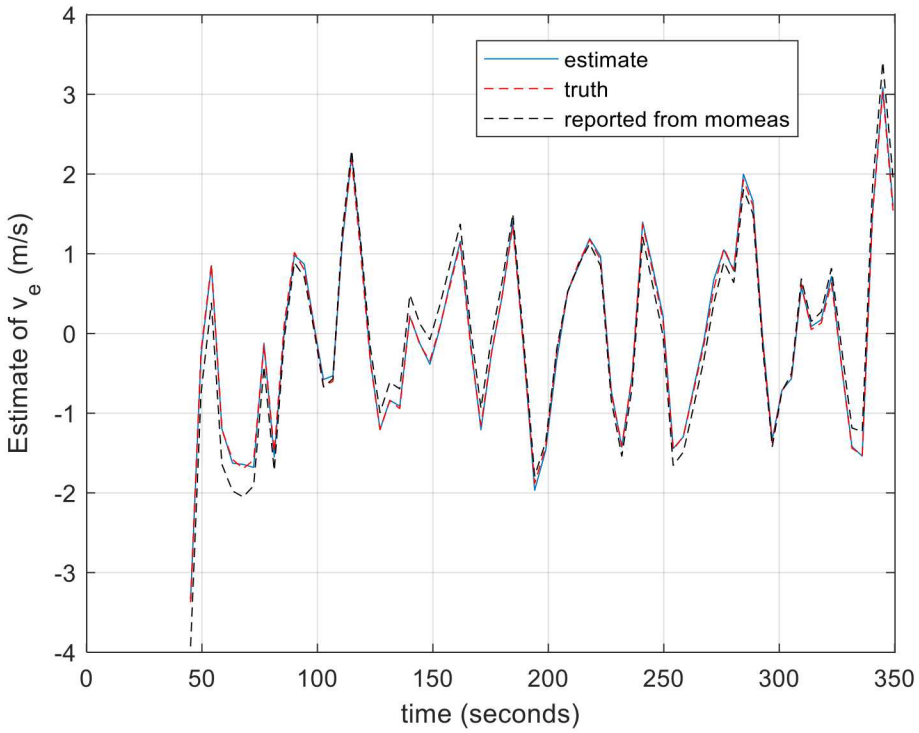

Figure 16. Estimate of v_e versus truth for case where 45 m offset and 0.25 m/s error is introduced into the reported motion measurement data

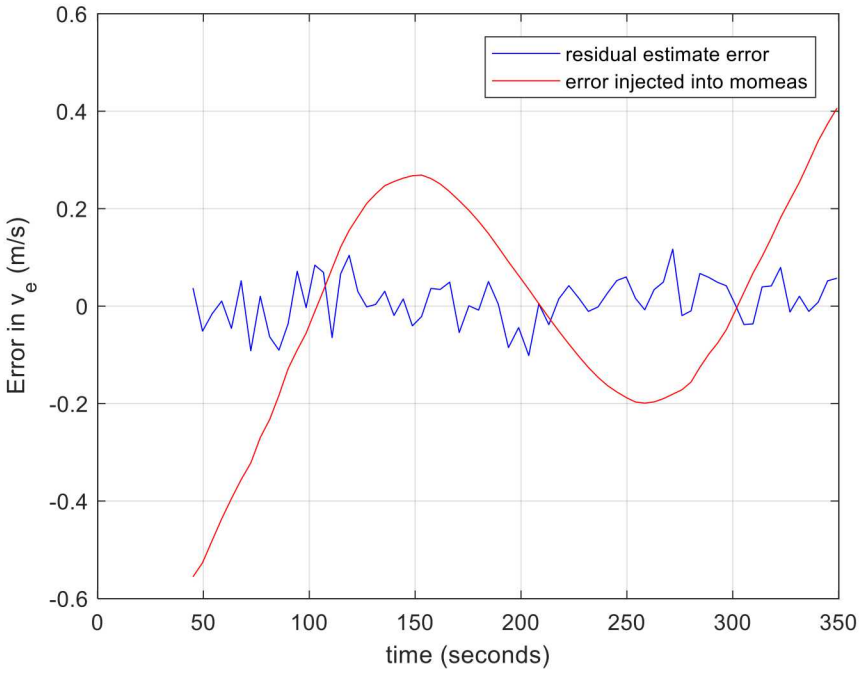

Figure 17. Injected motion measurement error in caused by v_e 45 m offset and 0.25 m/s error versus residual error after multiphase center v_e estimate

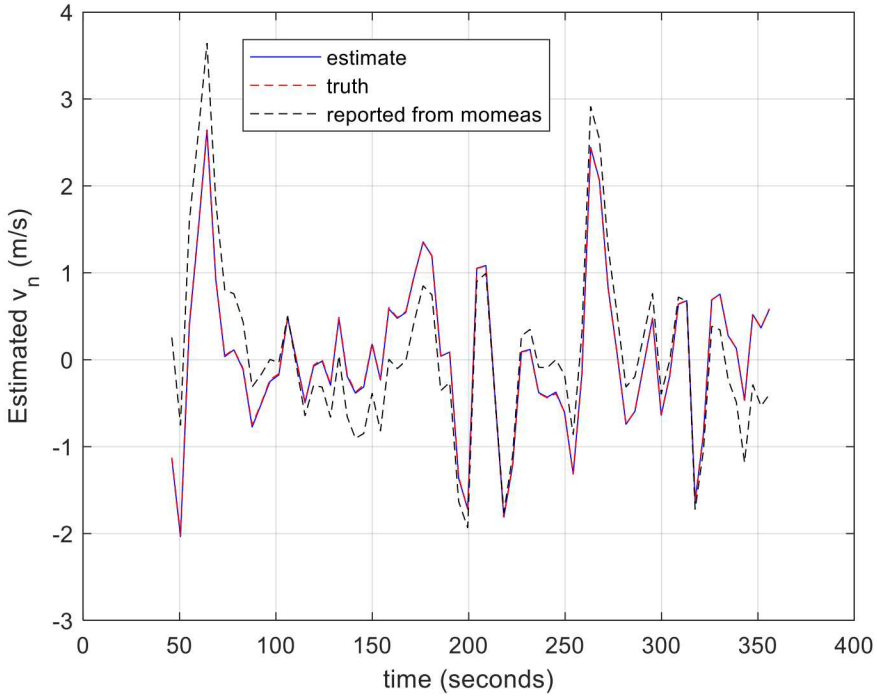

Figure 18. Estimate of v_n versus truth for case where 90 m offset and 0.5 m/s error is introduced into the reported motion measurement data

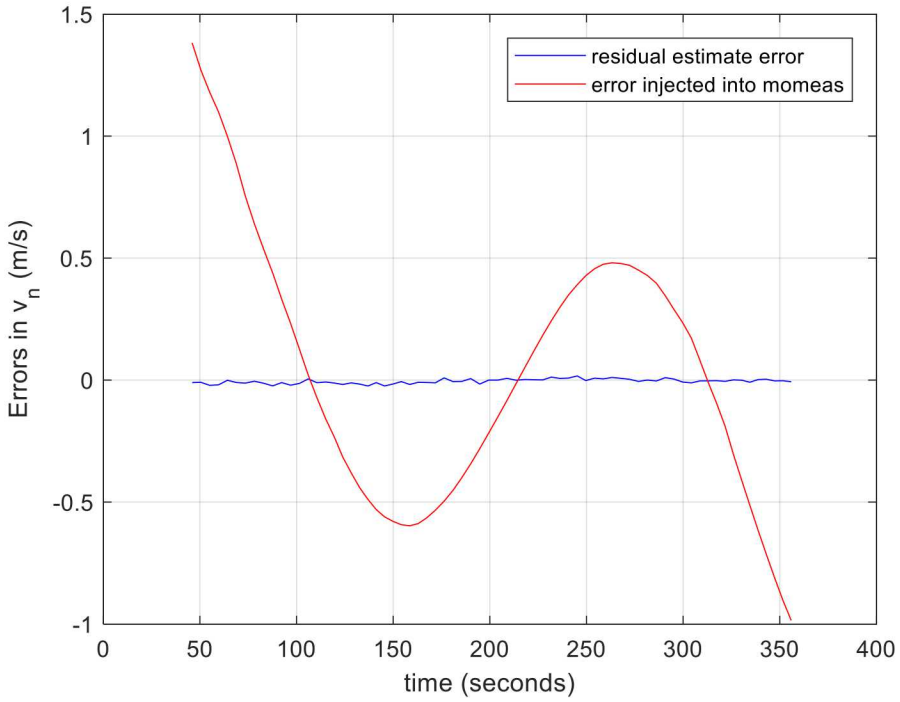

Figure 19. Injected motion measurement error in v_n caused by 90 m offset and 0.5 m/s error versus residual error in multiphase center v_n estimate

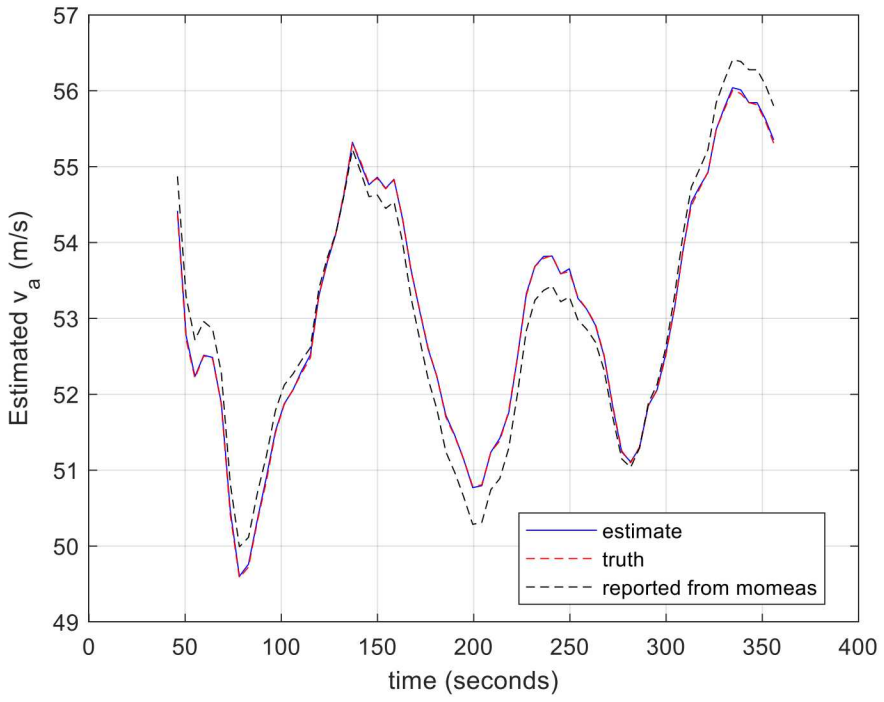

Figure 20. Estimate of v_a versus truth for case where 90 m offset and 0.5 m/s error is introduced into the reported motion measurement data

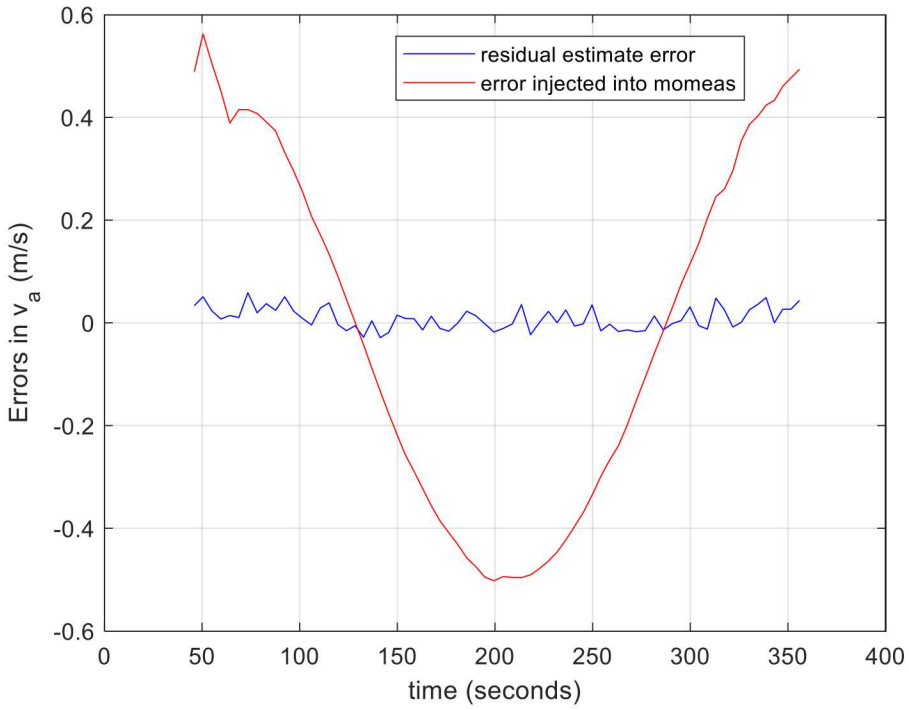

Figure 21. Injected motion measurement error in caused by v_a 90 m offset and 0.5 m/s error versus residual error after multiphase center v_a estimate

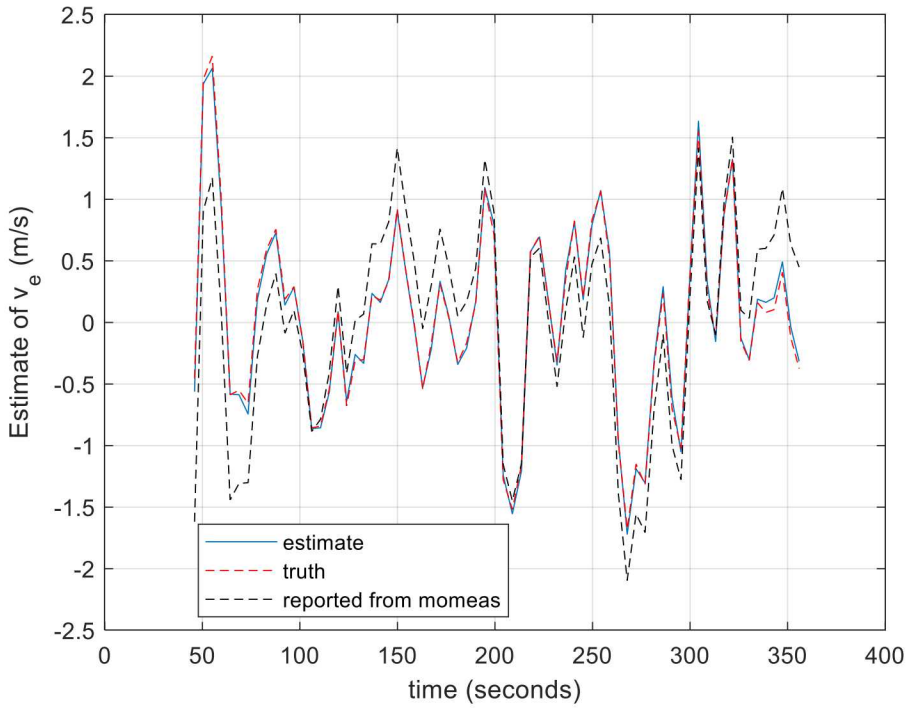

Figure 22. Estimate of v_e versus truth for case where 90 m offset and 0.5 m/s error is introduced into the reported motion measurement data

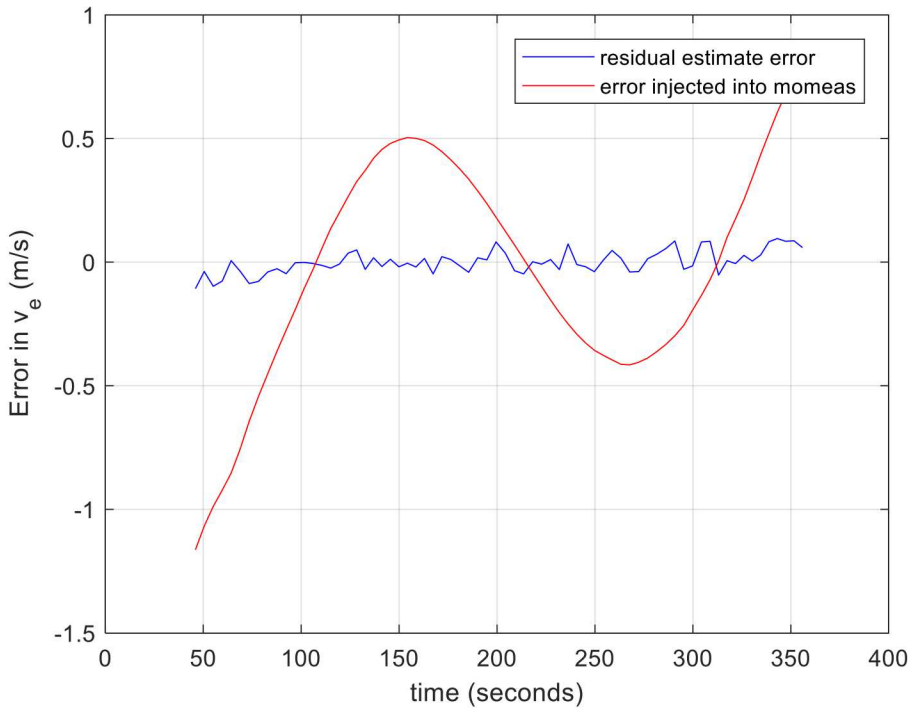

Figure 23. Injected motion measurement error in caused by v_e 90 m offset and 0.5 m/s error versus residual error after multiphase center v_e estimate

It doesn't matter how beautiful your theory is, it doesn't matter how smart you are. If it doesn't agree with experiment, it's wrong.

Richard P. Feynman

4. ERROR ANALYSIS

4.1. Error sources

There are various possible error sources to consider. For a well-designed radar, most of the error sources will be in the estimate of the angle information. Error sources for these can be found in many articles, and books published on interferometric techniques.

We will divide these up into calibration (bias) errors, and statistical errors and consider each in the following subsections.

4.2. Calibration

Calibration errors can be a significant error source in this method. We will briefly look at the impact of a couple of error sources. These include systematic RF path length differences and pointing bias. Another such error might be a scaling error in the interferometric baseline length. The particular experimental system used to collect the data discussed in this report requires a complex careful calibration of many terms. It is beyond the scope of this report to go into the details.

Assuming both errors are *small*, either a pointing bias and an RF path length difference effectively act like they are adding a small rotation to the antenna orientation. The result is that the we introduce a rotation into the estimated velocity error directions. For example, suppose we have a rotation error about the $\vec{u}_e$-axis (or nearly equivalently a calibration error phase error in $\Delta\Phi_a$), then this will in turn cause an error in the observed values $\left(\vec{u}_a \cdot \vec{u}_{r,n}\right)_{observed} \approx \left(\vec{u}_a \cdot \vec{u}_{r,n}\right)_{true} + \varepsilon$. The main effect will be an error in the estimated value of v_n by a coupling of the value of $v_a\varepsilon$. Note that since in our case v_a is approximately equal to the along-track velocity this error can be significant.

The effect of a baseline scaling error is straight forward in that it causes proportional scaling error in the estimated velocity (error).

4.3. Statistical Errors

In this section, we discuss the issues that affect the behavior of statistical errors in least squares methods. In least-squares the solution of the estimate of the velocities will have error variance proportional to the noise in the input variables, and inversely proportional to the total number of samples used to estimate the velocities, and the true angle spread of the scene content used to estimate the velocities. In other words, we want to use targets spread across the entire (hopefully relatively large) beamwidths in both elevation and azimuth[9]. If the target angle spread is small, then the least-squares problem is not well-conditioned leading to noisier velocity estimates.

The input noise in this case is mostly coming in through errors in the estimated target direction-of-arrival, i.e., the right-hand-side of equation (9). The noise in these values can be found in standard interferometric radar papers, and is known to be inversely proportional to the interferometric baseline length, the target signal-to-noise ratio, and the number of samples used in the phase estimation multilook process.

[9] We note that a large beamwidth can play against the desired higher signal-to-noise ratio. Also, it plays against our assumption that allowed us to linearize the least-squares solution.

4.4. Other Considerations

We previously mention a few considerations for the implementation and limits of this technique. We briefly repeat some of these here along with some additional considerations.

Probably one of the main considerations is that in practice we need to know the antenna orientation relative to some desired coordinate system, e.g., earth-centered earth-fixed (ECEF), in order to relate our estimated velocities to the desired coordinate system. We note that the velocity estimates in this technique are related to the antenna orientation.

We have already mentioned the issue of calibration, but wish to emphasize the fact that this technique requires very careful calibration and maintenance of calibration of the radar system, above what is typically required for an imaging radar, but such as is typically required for very accurate radar interferometers[10].

Also, we mentioned that this technique requires stationary target area, e.g., ocean waves are an issue. There is a possibility that we may be able to account for some limited ground traffic.

Finally, misfocus will have some effect on this technique due to loss of signal-to-noise ration and angular resolution; however, this technique has some robustness to misfocus due to the averaging.

[10] Note that we are not trying to scare off the reader, merely to emphasize the importance of such careful calibration as has been applied to other radar systems at Sandia and elsewhere.

5. POTENTIAL FUTURE WORK AND/OR ISSUES

This section briefly mentions a few desirable areas to pursue in the future. First, we would like to collect more data in other varying circumstances to test the robustness of this technique. One important area is that we would like to demonstrate the integration of this information in a real-time motion measurement Kalman filter implementation during our test flights. This could include trade-offs between the number of points integrated to form the range-Doppler image, and the time-lag of the estimates.

Also, we would like to further expand on system design and analysis in order to specify what system requirements are necessary and how this information would feed into a motion measurement system. Antenna sizes, power requirements, coherent processing interval lengths, and geometries for optimal operation should be investigated for the given application requirements.

“History is a guide to navigation in perilous times.”

David McCullough

6. CONCLUSIONS

We have presented a technique to estimate the 3D velocity of a moving radar platform using multiple radar subarrays. This document extends the work in [1]. We also show favorable results in 3-D velocity using this technique with data collected from the Sandia testbed radar. The results do not use target position knowledge.

REFERENCES

[1] A. W. Doerry, V. Horndt, D. L. Bickel, and R. M. Naething, "Estimating Radar Velocity using Direction of Arrival Measurements", *SAND Report SAND2014-17277*, Sep. 2014.

[2] G. Strang, *Linear Algebra and its Applications*, 4th Ed., 2006.

[3] M. I. Skolnik, *Introduction to Radar Systems*, 2nd Ed., McGraw Hill Co., 1981.

[4] D. Eberly, "Least Squares Fitting of Data by Linear or Quadratic Structures", https://www.geometrictools.com/Documentation/LeastSquaresFitting.pdf, 2019.

DISTRIBUTION

Email—Internal

Name	Org.	Sandia Email Address
R. A. Gonzales	05300	ragonza@sandia.gov
B. L. Tise	05300	bltise@sandia.gov
J. A. Payne	05320	japayne@sandia.gov
S. Rodriguez	05322	srodrig@sandia.gov
S. Jenkins	05322	sjenki@sandia.gov
S. Castillo	05340	spcasti@sandia.gov
B. L. Burns	05340	blburns@sandia.gov
B. G. Rush	05342	bgrush@sandia.gov
T. P. Bielek	05342	tpbiele@sandia.gov
J. A. Rohwer	05342	jarohwe@sandia.gov
D. G. Thompson	05342	dgthomp@sandia.gov
M. E. Thompson	05342	mthomp2@sandia.gov
M. McCandless	05343	mmccand@sandia.gov
W. H. Hensley	05344	whhensl@sandia.gov
B. Conder	05344	bconder@sandia.gov
R. M. Naething	05344	rmnaeth@sandia.gov
A. M. Raynal	05344	amrayna@sandia.gov
K. W. Sorensen	05345	kwsoren@sandia.gov
M. Diltz	05346	madiltz@sandia.gov
D. A. Yocky	05346	dayocky@sandia.gov
L. M. Klein	05346	lklein@sandia.gov
R. D. West	05346	rdwest@sandia.gov
D. M. Small	05348	dmsmall@sandia.gov
M. R. Lewis	05349	mrlewis@sandia.gov
A. W. Doerry	05349	awdoerr@sandia.gov
J. Topolski	05349	jatopol@sandia.gov
Technical Library	01177	libref@sandia.gov
D. L. Bickel	05344	dlbicke@sandia.gov

This page left blank

Sandia National Laboratories

Sandia National Laboratories is a multimission laboratory managed and operated by National Technology & Engineering Solutions of Sandia LLC, a wholly owned subsidiary of Honeywell International Inc. for the U.S. Department of Energy's National Nuclear Security Administration under contract DE-NA0003525.